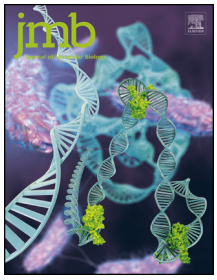

Divalent Cations Alter the Rate-Limiting Step of PrimPol-Catalyzed DNA Elongation

Wenyan Xu[1], Wenxin Zhao[1], Nana Morehouse[1], Maya O. Tree[1] and Linlin Zhao[1,2]

1 - Department of Chemistry and Biochemistry, Central Michigan University, Mount Pleasant, MI 48859, USA
2 - Biochemistry, Cellular and Molecular Biology Graduate Program, Central Michigan University, Mount Pleasant, MI 48859, USA

Correspondence to Linlin Zhao: *Department of Chemistry and Biochemistry, Central Michigan University, Biosciences 4112, Mount Pleasant, MI 48859, USA. linlin.zhao@cmich.edu*
https://doi.org/10.1016/j.jmb.2019.01.002
Edited by James Berger

Abstract

PrimPol is the most recently discovered human DNA polymerase/primase and plays an emerging role in nuclear and mitochondrial genomic maintenance. As a member of archaeo-eukaryotic primase superfamily enzymes, PrimPol possesses DNA polymerase and primase activities that are important for replication fork progression *in vitro* and *in cellulo*. The enzymatic activities of PrimPol are critically dependent on the nucleotidyl-transfer reaction to incorporate deoxyribonucleotides successively; however, our knowledge concerning the kinetic mechanism of the reaction remains incomplete. Using enzyme kinetic analyses and computer simulations, we dissected the mechanism by which PrimPol transfers a nucleotide to a primer-template DNA, which comprises DNA binding, conformational transition, nucleotide binding, phosphoester bond formation, and dissociation steps. We obtained the rate constants of the steps by steady-state and pre-steady-state kinetic analyses and simulations. Our data demonstrate that the rate-limiting step of PrimPol-catalyzed DNA elongation depends on the metal cofactor involved. In the presence of Mn^{2+}, a conformational transition step from non-productive to productive PrimPol:DNA complexes limits the enzymatic turnover, whereas in the presence of Mg^{2+}, the chemical step becomes rate limiting. As evidenced from our kinetic and simulation data, PrimPol maintains the same kinetic mechanism under either millimolar or physiological micromolar Mn^{2+} concentration. Our study revealed the underlying mechanism by which PrimPol catalyzes nucleotide incorporation with two common metal cofactors and provides a kinetic basis for further understanding the regulatory mechanism of this functionally diverse primase-polymerase.

Introduction

Complete and accurate genome duplication is essential for passing on genetic information to the next-generation cells. Unfortunately, DNA lesions or non-canonical DNA structures constantly challenge DNA replication [1,2]. The stressed replication can be rescued by one or more of the following mechanisms: (i) DNA damage avoidance [3], (ii) specialized DNA polymerases (pols) copying past the obstructive DNA structures, and (iii) replication restart after the roadblock [4,5]. The lesion bypass (also known as translesion synthesis) is coordinated by specialized DNA polymerases and accessory proteins, and can occur at the fork or post-replicatively [6–11]. The enzyme involved in the replication reinitiation process in eukaryotes was unknown until the recent discovery of a bifunctional primase-polymerase, PrimPol [12–16].

PrimPol belongs to the archaeo-eukaryotic primase (AEP) superfamily enzymes. The homologs of human PrimPol are present in many eukaryotic organisms, such as animals, plants, fungi, and protists, but is absent in organisms, such as *Drosophila melanogaster*, *Caenorhabditis elegans*, and *Saccharomyces cerevisiae* [13,17,18]. PrimPol is the second AEP superfamily enzyme found in humans, aside from the pol α-associated DNA primase subunit, Prim1 or p49. PrimPol is a versatile enzyme that can catalyze *de novo* DNA synthesis or lesion bypass using dNTPs substrates [12,13,15,16]. The primase activity of PrimPol is important for rescuing the stalled DNA

replication *in vitro* and *in cellulo* [13,15,16,19,20]. In avian DT40 cells, PrimPol-mediated re-priming is required to tolerate chain-terminating nucleotide analogs, replication-blocking DNA lesions [21], or structural impediments like G-quadruplexes [19]. PrimPol can also contribute to mitochondrial DNA maintenance by restarting the stressed mitochondrial DNA replication or repriming from nonconventional origins [13,20]. Furthermore, PrimPol exerts anti-mutagenic activities on the leading strand during somatic hypermutation in mouse, presumably *via* its primase activity [22]. Although the biological importance of its translesion synthesis polymerase activity remains to be established, PrimPol can perform low-fidelity DNA synthesis across several DNA lesions *in vitro* [12,13,23]. Collectively, this body of research underscores the importance of PrimPol for both nuclear and mitochondrial DNA maintenance particularly under stressed conditions.

PrimPol is a 560-amino-acid protein that has an N-terminal AEP-like catalytic domain and a C-terminal zinc finger domain. The catalytic domain is responsible for the nucleotidyl transferase activity of PrimPol, and the zinc finger domain facilitates the binding and selection of the 5′-nucleotide of the newly synthesized primer and the recognition of preferred initiation sites [24]. The C-terminal domain also includes crucial motifs that interact with replication protein A (RPA) [25]. Structural data have revealed that the catalytic domain of PrimPol (residues 1–354) comprises N-helix, module N (residues 35 to 105), and module C (residues 108 to 200 and 261 to 348) regions connected by flexible linkers [26]. The module C region contains active site residues and encompasses the functions of both the finger and palm domains of other DNA polymerases. The module N and N-helix regions interact with the template strand but exhibit fewer contacts relative to most other DNA polymerases. Notably, PrimPol has almost no contact with the DNA primer strand, in contrast with the thumb domain of other DNA polymerases gripping the primer. The lack of interactions with the primer strand corroborates PrimPol's distributive property and its ability to synthesize DNA without an existing primer. Together, the unique structural features suggest that PrimPol may employ an unconventional mechanism for DNA polymerization.

The kinetic mechanism which by PrimPol catalyzes the nucleotidyl-transfer reaction remains an important unanswered question. Although partial kinetic characterizations have been reported [23,27,28], a complete kinetic pathway of PrimPol-mediated DNA elongation and the rate-limiting step(s) of the reaction are unknown. Such information is not only fundamental for further understanding the enzymatic activities of PrimPol and other primase-polymerases, but also useful for exploring novel approaches to modulate PrimPol's activities for biotechnological or therapeutic applications [25,29,30]. In this study, we conducted in-depth kinetic analyses and computer simulations to dissect the elemental steps of PrimPol's DNA polymerase activity. Our data demonstrate that the enzymatic turnover of PrimPol is limited by the chemical step in the presence of Mg^{2+} or a conformational transition step in the presence of Mn^{2+}. We constructed a minimal kinetic model and obtained the rate constants of the encompassing steps by enzyme kinetic analyses and simulations. Together, our study provides mechanistic insight into the kinetic basis for PrimPol and suggest a critical role of divalent metal ions in regulating PrimPol's catalytic properties.

Results

Optimization of assay conditions

First, we assessed the DNA binding activity of the recombinant PrimPol by determining its equilibrium dissociation constant ($K_{d,DNA}$) using a 13/28-mer primer-template DNA substrate (hereinafter referred to as DNA; sequence shown in Table S1). The $K_{d,DNA}$ is 145 (± 27) nM in the presence of 2 mM Mn^{2+} (Fig. 1a) and 1050 (± 110) nM in the presence of 5 mM Mg^{2+} (Fig. S2C) from fluorescence polarization experiments. The $K_{d,DNA}$ values obtained without metal cofactors or with 20 μM Mn^{2+} are comparable to the $K_{d,DNA}$ under 2 mM Mn^{2+} (Fig. S2A and B), suggesting that it is the identity of the cofactor (Mn^{2+} *versus* Mg^{2+}) rather than its concentration affecting PrimPol's DNA-binding ability. Our observations are consistent with the attenuated DNA-binding activities of PrimPol with Mg^{2+} reported previously [23,27,28]. PrimPol is predicted to be unstable by the ProtParam tool [31]; therefore, we evaluated how PrimPol's DNA polymerase activity changes with time or in the presence of different reaction components. We calculated the half-life of PrimPol based on the change of the observed rate constant ($k_{obs,m} = V_0/[E]$) of single-nucleotide incorporation under steady-state kinetic conditions (20 μM DNA-13/28, 0.1 μM PrimPol, and excess dTTP). The half-life is 36, 14, or 7 min, when the enzyme was incubated alone, with DNA, or with DNA and 2 mM $MnCl_2$, respectively, in 50 mM Hepes (pH 7.4) at 37 °C (Fig. 1b). The short half-life of PrimPol is consistent with its rapid heat-inactivation observed previously [32]. Therefore, the reaction time of subsequent assays was kept within a few minutes to avoid a dramatic change in enzymatic activity during the reaction except for a few steady-state kinetic experiments.

Next, we examined the DNA polymerase activity of PrimPol as a function of salt, DNA, or metal concentration. The DNA polymerase activity decreased with an increasing concentration of NaCl (Fig. 1c), likely due

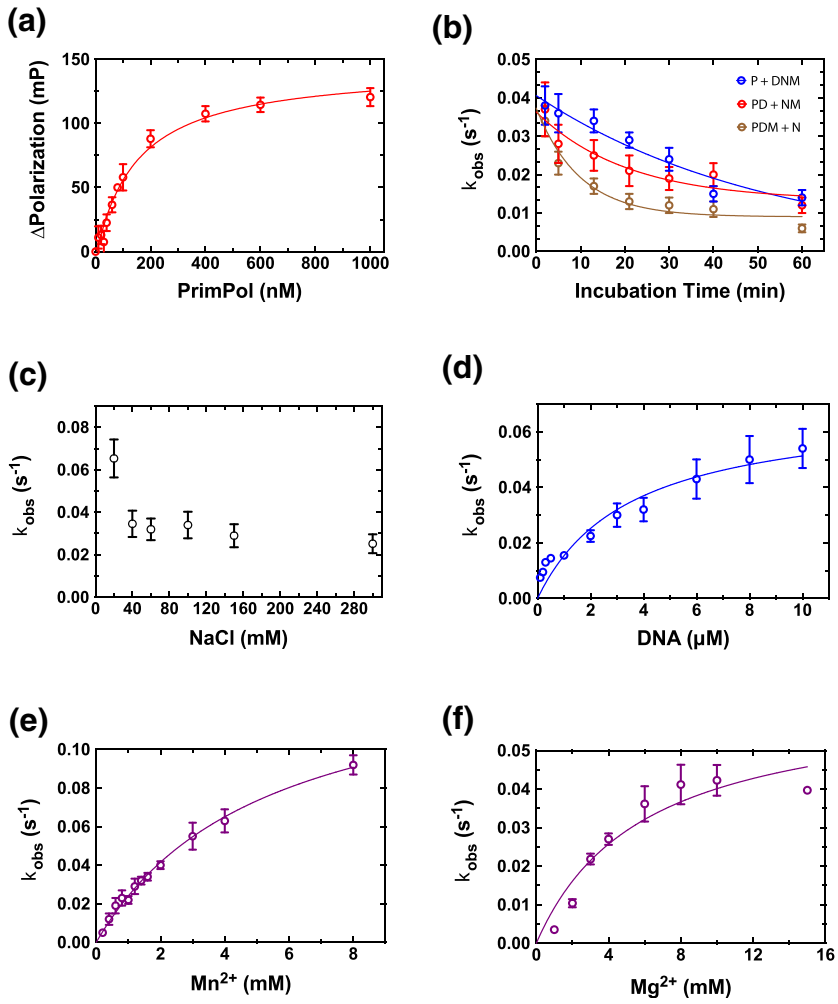

Fig. 1. Characterization of the DNA-binding activity of PrimPol and optimization of assay conditions. The enzyme activity is assessed by the observed rate constant ($k_{obs,m} = V_0$/[E]) of single-nucleotide incorporation. (a) The equilibrium dissociation constant ($K_{d,DNA}$) of PrimPol from fluorescence polarization assays. Data were fit to a quadratic equation (Eq. (1)) to provide a $K_{d,DNA}$ of 145 (± 27) nM in the presence of 2 mM Mn^{2+}. The number in parentheses is the S.E. of the fitting. Error bars indicate the range of data from two experiments. (b) The stability of PrimPol in the presence of different reaction components, assessed from the change of $k_{obs,m}$ as a function of pre-incubation time, fit to a single exponential decay equation (Eq. (2)). PrimPol (*P*) was pre-incubated for varying times alone (blue circle), with DNA (*D*, red circle), or with DNA and $MnCl_2$ (*M*, brown circle) before the addition of dNTP (*N*) to initiate the reaction. (c) Effect of salt concentration on $k_{obs,m}$. (d) DNA concentration-dependent reactions in the presence of 200 μM dTTP and 2 mM $MnCl_2$ to yield a $K_{m,DNA}$ of 3.6 (± 1.0) μM. (e) Mn^{2+}-dependent reactions in the presence of 200 μM dTTP and 20 μM DNA to obtain a $K_{m,Mn}$ of 5.3 (± 0.4) mM. (f) Mg^{2+}-dependent reactions in the presence of 200 μM dTTP and 20 μM DNA to obtain a $K_{m,Mg}$ of 5.9 (± 2.4) mM. Numbers in parentheses refer to the S.E. of the fitting. Error bars in panels b through f are S.D. ($n \geq 3$).

to compromised electrostatic interactions between PrimPol and DNA. PrimPol's polymerase activity increased hyperbolically with DNA concentration, revealing a $K_{m,DNA}$ of 3.6 μM (Fig. 1d). Therefore, we used a medium salt concentration (50 mM) and a saturating DNA concentration (20 μM) in subsequent assays. We also evaluated the metal concentration dependency of PrimPol-catalyzed nucleotide insertion. Mn^{2+} has been considered as the preferred metal cofactor for PrimPol [12,13,15,23,33], although *in vivo* the importance of Mn^{2+} for PrimPol catalysis remains to be established. We measured $k_{obs,m}$ under varying concentrations of Mn^{2+} or Mg^{2+} ions, and fit the data to a hyperbolic equation. The K_m is 5.3 mM for Mn^{2+} (Fig. 1e) and 5.9 mM for Mg^{2+} (Fig. 1f). The typical intracellular concentration of Mn^{2+} is in the micromolar range [34], but can accumulate in certain tissues and subcellular compartments [35,36]. The total Mg^{2+} concentration in mammalian cells ranges from 17 to 20 mM, with 5%–20% of the ions in the free form [37]. Therefore, we conducted kinetic experiments under three different conditions, that is, 2 mM Mn^{2+}, 50 μM Mn^{2+}, and 2 mM Mg^{2+}. Together, these experiments established the appropriate assay conditions for subsequent kinetic characterizations.

PrimPol-catalyzed DNA elongation entails a rate-limiting step at or prior to chemistry

To decipher the rate-limiting step of PrimPol-mediated DNA polymerization, we carried out in-depth enzyme kinetic analyses. Steady-state kinetic experiments revealed a turnover number (k_{cat}) of 0.05 s^{-1} and a Michaelis constant ($K_{m,dTTP}$) of 14 μM in the presence of 2 mM Mn^{2+} (Table 1 and Fig. S3A), similar to published data [23]. Lowering Mn^{2+} to 50 μM resulted in a moderate decrease (4-fold) in PrimPol's catalytic proficiency ($k_{cat}/K_{m,dTTP}$) relative to that obtained with 2 mM Mn^{2+}, indicating that PrimPol retains its enzyme efficiency under micromolar Mn^{2+}. On the other hand, substituting Mn^{2+} with 2 mM Mg^{2+} led to a dramatic decrease

(150-fold) in PrimPol's overall catalytic proficiency owing to a high $K_{m,dTTP}$ of 430 μM, consistent with the general perception that Mg^{2+} is a less effective metal cofactor for PrimPol's catalysis.

To understand the elementary steps in the reaction pathway, we carried out several pre-steady-state kinetic experiments. First, we performed "burst" kinetics using excess DNA (30 μM) and limiting PrimPol (5 or 10 μM, Fig. 2a) to ensure that nearly all the enzyme molecules are bound to DNA substrates on the basis of $K_{d,DNA}$. In the presence of 2 mM Mn^{2+}, whereby highest catalytic proficiency was observed in steady-state kinetics, product formation lacked a burst phase and yielded a linear time course (Fig. 2b and c). The lack of burst kinetics is not due to the suboptimal DNA binding activity of the preparation, as verified by fluorescence titration experiments (Fig. S1). The observation suggests that PrimPol-catalyzed nucleotide incorporation contains a rate-limiting step at or before the chemical step.

Furthermore, we used single-turnover kinetic assays (excess PrimPol relative to DNA) to obtain the maximal polymerization rate (k_{pol}) of PrimPol and the apparent equilibrium dissociation constant of nucleotide ($K_{d,dNTP}$). The macroscopic rate constant (k_{pol}) includes contributions from the rate of nucleotide binding, the potential conformational change of ternary complexes (PrimPol:DNA:dNTP), and the nucleotidyl-transfer reaction [38]. The observed rate constants from the exponential time courses (Fig. 3b) increased hyperbolically with dTTP concentration (Fig. 3c), revealing a k_{pol} of 0.12 s^{-1} and a $K_{d,dTTP}$ of 6.1 μM in the presence of 2 mM Mn^{2+}, as summarized in Table 2. Lowering Mn^{2+} concentration to 50 μM did not appear to affect k_{pol} (0.11 s^{-1}) but slightly increased $K_{d,dTTP}$ (14 μM; Fig. S3 and Table 2), suggesting that the concentration of manganese does not significantly alter the nucleotide binding and chemistry steps. Compared to Mn^{2+}-dependent reactions, single-turnover reactions with Mg^{2+} revealed a modest decrease in k_{pol} (0.056 s^{-1}) and a significant increase in $K_{d,dTTP}$ (430 μM; Fig. S4 and Table 2), indicating a compromised nucleotide binding process. The composite data clearly demonstrate different thermodynamic and kinetic properties of PrimPol in the presence of two different divalent cations and strongly suggest that a rate-limiting step proceeds or occurs at the chemical step for PrimPol-catalyzed DNA elongation.

Table 1. Steady-state kinetic parameters of PrimPol-catalyzed dTTP incorporation with different DNA substrates in the presence of Mn^{2+} or Mg^{2+}

DNA	Metal	k_{cat} (s^{-1})	$K_{m,dTTP}$ (μM)	k_{cat}/K_m (s^{-1} μM^{-1})
DNA-13/28	2 mM Mn^{2+}	0.050 ± 0.003	14 ± 2	0.0036
	50 μM Mn^{2+}	0.020 ± 0.002	24 ± 6	0.00083
	2 mM Mg^{2+}	0.010 ± 0.001	430 ± 90	0.000023

Errors are S.E. derived from fitting of nucleotide concentration dependencies to a hyperbolic equation (Eq. (3)).

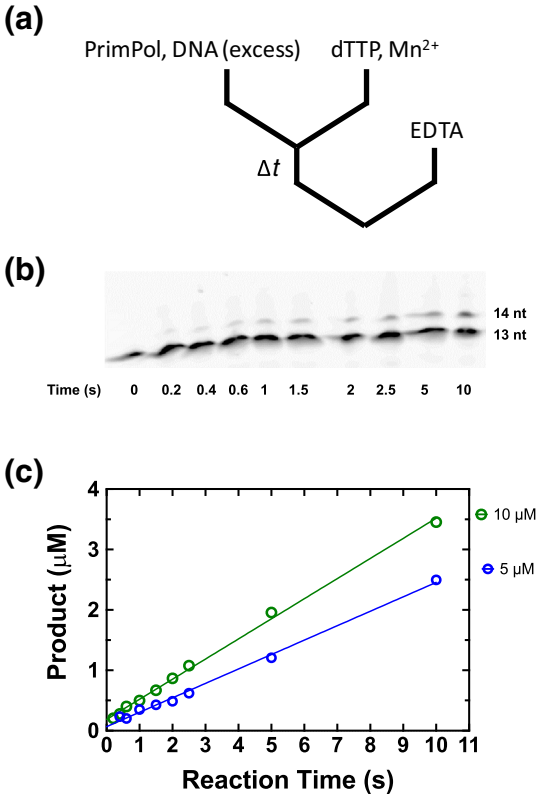

Fig. 2. PrimPol-catalyzed nucleotide insertion lacks "burst" kinetics. (a) Schematic illustration of the sequential mixing of different reaction components under "burst" kinetic conditions, that is, excess DNA (30 μM), limiting PrimPol (10 μM), and 2 mM Mn^{2+}. (b) Representative gel image of single-nucleotide incorporation with 10 μM PrimPol. (c) Product formation time courses in the presence of 5 μM or 10 μM PrimPol. More than 99% of PrimPol forms PrimPol:DNA complexes on the basis of $K_{d,DNA}$ under the current condition.

The rate-limiting step varies depending on the metal cofactor

To decipher whether the phosphoester bond formation is rate limiting, we examined the thio-effects of PrimPol-catalyzed nucleotide incorporation using an analog [(α)*S*-dTTP] with the non-bridging oxygen at the α-phosphate substituted with a sulfur atom relative to the unmodified dTTP. Historically, sulfur-substituted nucleotide analogs have been used to assess whether the chemical step is rate limiting under single-turnover conditions [39–41]. Because sulfur is less electronegative than oxygen, a decrease in the nucleotide incorporation rate is expected with (α)*S*-dTTP (relative to dTTP), if the phosphoester

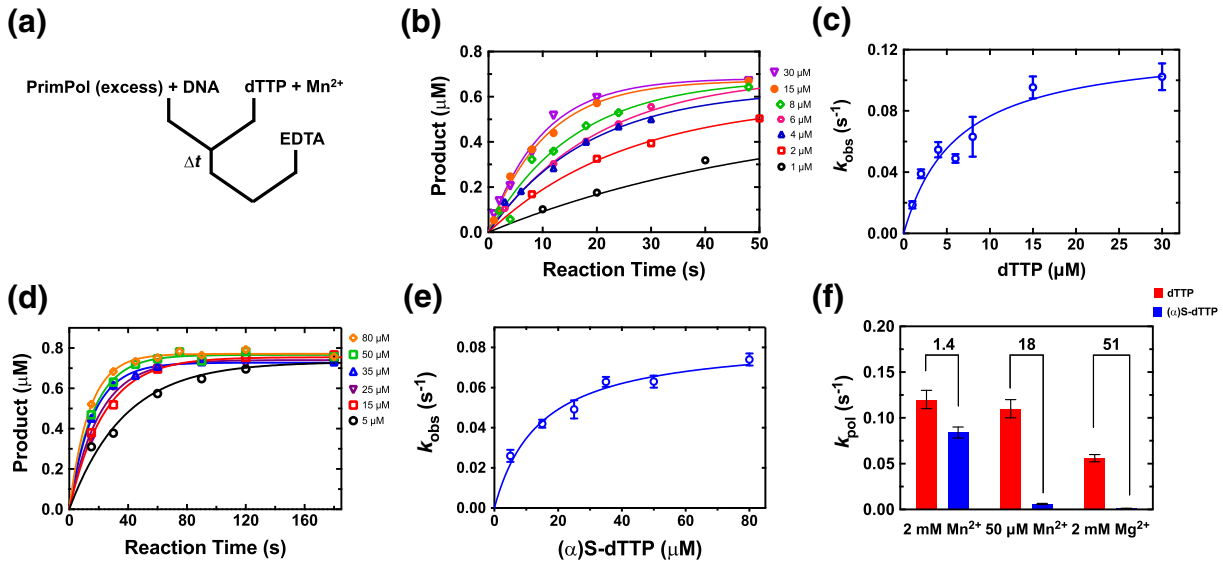

Fig. 3. Single-turnover kinetics of PrimPol-catalyzed nucleotide incorporation with dTTP or (α)*S*-dTTP. (a) Schematic illustration of the sequential mixing of different reaction components. Assays contained PrimPol (4 μM), DNA (0.8 μM), $MnCl_2$ (2 mM), and varying concentrations of dTTP or (α)*S*-dTTP. Single exponential (Eq. (4)) time courses are shown in panel b with dTTP and in panel d with (α)*S*-dTTP. In panels c and e, the observed rate constants from the exponential time courses are fit to a hyperbolic equation (Eq. (5)) to obtain k_{pol} and $K_{d,dTTP}$ (summarized in Table 2). Error bars in panels b and d are S.E. of the fitting. Representative gel images are shown in Fig. S8. (f) Comparison of k_{pol} values under different metal conditions. Data obtained with 2 mM Mg^{2+} or 50 μM Mn^{2+} are derived from Supplemental Figs. S3 and S4. Errors are S.E. of the fitting. Two k_{pol} values in each set are statistically different according to the two-way ANOVA comparison.

bond formation is rate limiting. In the presence of 2 mM Mg^{2+}, a significant elemental effect was observed ($k_{pol,dTTP}/k_{pol,\ \alpha\text{-}(\alpha)S\text{-}dTTP}$, 51, shown in Table 2 and Fig. S4), suggesting that the chemical step can be rate limiting under such conditions. Conversely, in the presence of 2 mM Mn^{2+}, a weak thio-effect was observed ($k_{pol,dTTP}/k_{pol,\ \alpha\text{-}(\alpha)S\text{-}dTTP}$, 1.4; Fig. 3 and Table 2), suggesting that the chemical step is unlikely to be rate limiting. With 50 μM Mn^{2+}, a modest thio-effect was obtained ($k_{pol,dTTP}/k_{pol,\ \alpha\text{-}(\alpha)S\text{-}dTTP}$, 18; shown in Table 2 and Fig. S3), which precluded definitive interpretations of the elemental effect. The full magnitude of the thio-effect can range from 10 to 100 depending on electronic and steric factors and the nature of the transition state, which makes interpretation of moderate thio-effects controversial [38,42,43]. In addition, under subsaturating Mn^{2+} (50 μM) concentration (relative to nucleotide substrate), the binding of Mn^{2+} to the phosphate group of nucleoside triphosphate or oligodeoxynucleotides [44] could significantly decrease the available metal ions for catalysis (evidenced by the decrease of k_{obs} when (α)*S*-dTTP exceeds 30 μM in Fig. S3D). Nevertheless, different elemental effects observed under millimolar Mn^{2+} and Mg^{2+} suggest that the rates of the chemical step vary considerably, consistent with different k_{cat} and k_{pol} values observed under the two conditions (Tables 1 and 2). Therefore, our data argue the presence of a rate-limiting non-chemical step before chemistry in the presence of

Table 2. Single-turnover kinetic parameters of PrimPol-catalyzed dTTP incorporation

DNA	Metal	Nucleotide	k_{pol} (s^{-1})	$K_{d,dNTP}$ (μM)	$k_{pol,dTTP}/k_{pol,\ \alpha\text{-}(\alpha)S\text{-}dTTP}$
DNA-13/28	2 mM Mn^{2+}	dTTP	0.12 ± 0.01	6.1 ± 1.8	1.4
		(α)*S*-dTTP	0.084 ± 0.006	14 ± 3.2	
	50 μM Mn^{2+}	dTTP	0.11 ± 0.01	14 ± 3.0	18
		(α)*S*-dTTP	0.0060 ± 0.0006	4.8 ± 1.7	
	2 mM Mg^{2+}	dTTP	0.056 ± 0.004	430 ± 80	51
		(α)*S*-dTTP	0.0011 ± 0.0002	120 ± 70	

Errors are S.E. derived from fitting of nucleotide concentration dependencies to a hyperbolic equation (Eq. (5)).

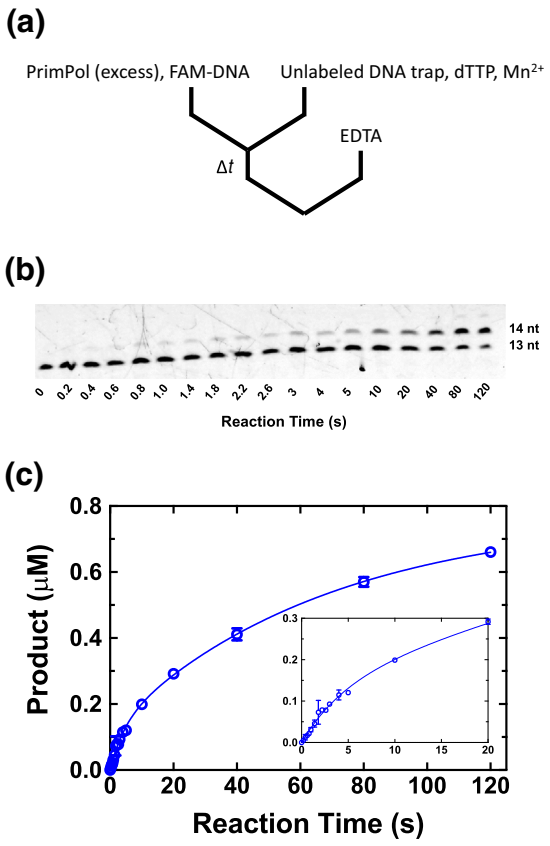

Fig. 4. Biphasic kinetics of PrimPol-catalyzed nucleotide incorporation in the presence of 2 mM Mn^{2+}. (a) Schematic illustration of the sequential mixing of different reaction components. (b) Representative gel image of the single-nucleotide insertion to form 14-mer products. (c) Biphasic kinetic time course is fit to a double exponential equation (Eq. (6)) with data summarized in Table 3. Data represent the mean from two experiments; error bars show the ranges of data.

2 mM Mn^{2+} and a rate-limiting chemical step in the presence of 2 mM Mg^{2+}, implying a regulatory role of metal cofactors for PrimPol-mediated DNA synthesis.

A conformational transition limits PrimPol's turnover in the presence of millimolar Mn^{2+}

To further pinpoint the non-chemical, rate-limiting step of PrimPol-catalyzed primer extension in the presence of 2 mM Mn^{2+}, we performed a DNA trapping experiment under single-turnover conditions. Similar assays have been used to capture the non-productive enzyme:DNA complexes for other polymerases [45,46]. An equilibrated solution of PrimPol and FAM-labeled DNA was mixed with a solution of dTTP, Mn^{2+}, and a large molar excess of the unlabeled DNA trap. Reaction was allowed for varying times before quenching with EDTA (Fig. 4a). Upon mixing with the DNA trap, any PrimPol molecules that were not in complex with the labeled DNA would bind to the DNA trap. The time course of the single-nucleotide incorporation revealed a biphasic kinetic profile—a fast phase followed by a slow phase (Fig. 4b and c), suggesting that there are at least two types of PrimPol:DNA complexes that can eventually be converted to extended primers. The fast phase demonstrates the existence of productive PrimPol:DNA complexes that catalyze the product formation rapidly, whereas the slow phase corresponds to a gradual transition from non-productive to productive complexes without PrimPol dissociating from DNA. We reason that these co-existing complexes are binary complexes (PrimPol:DNA) rather than ternary complexes (PrimPol:DNA:dNTP), because if different complexes appear upon dNTP binding, a single-phase product formation would have been observed.

The biphasic data were fit to a double exponential equation, resulting in a fast rate of 0.23 s^{-1} with an amplitude of 16% and a slow rate of 0.015 s^{-1} with an amplitude of 84%, relative to the total product formed (Table 3). The overall amplitude (0.77 μM) is in excellent agreement with the total amount of pre-formed PrimPol:DNA complexes (0.80 μM) calculated from $K_{d,DNA}$ using Eq. (7). The biphasic kinetics indicates that for primer extension, PrimPol binds to DNA substrates to form both productive and non-productive complexes. The slow phase, correlating to a conformational transition from non-productive to productive complexes, occurs at a rate (0.015 s^{-1}) that is comparable to k_{cat} (0.050 s^{-1}), indicating that the conformational transition could limit the enzymatic turnover. Consequently, the conformational transition step was assigned to the rate-limiting step in the presence of millimolar Mn^{2+}. We also conducted the DNA trapping experiment for Mg^{2+}-dependent reactions and observed a single exponential time course (Fig. S6C), corroborating a rate-limiting chemical step in Mg^{2+}-dependent reactions. Reactions with 50 μM Mn^{2+} resulted in no product formation, likely due to the depletion of manganese ions for catalysis

Table 3. Biphasic kinetic parameters of PrimPol-catalyzed dTTP incorporation derived from Fig. 4

	A_{fast} (nM)	k_{fast} (s^{-1})	A_{slow} (nM)	k_{slow} (s^{-1})	A_{fast}/A_{total} (%)
DNA-13/28	120 ± 20	0.23 ± 0.04	650 ± 20	0.015 ± 0.002	16

Data are mean from two independent experiments. Errors are S.E of the fit to a double-exponential equation (Eq. (6)).

caused by binding of Mn^{2+} to the DNA trap (35 μM) [44]. Taken together, these results support the distinct roles of different divalent cations for PrimPol and revealed a rate-limiting conformational transition step for PrimPol under millimolar Mn^{2+}.

Kinetic mechanism of PrimPol obtained with global fitting and simulations

Guided by our kinetic data, we propose a minimal kinetic model for PrimPol-catalyzed DNA elongation,

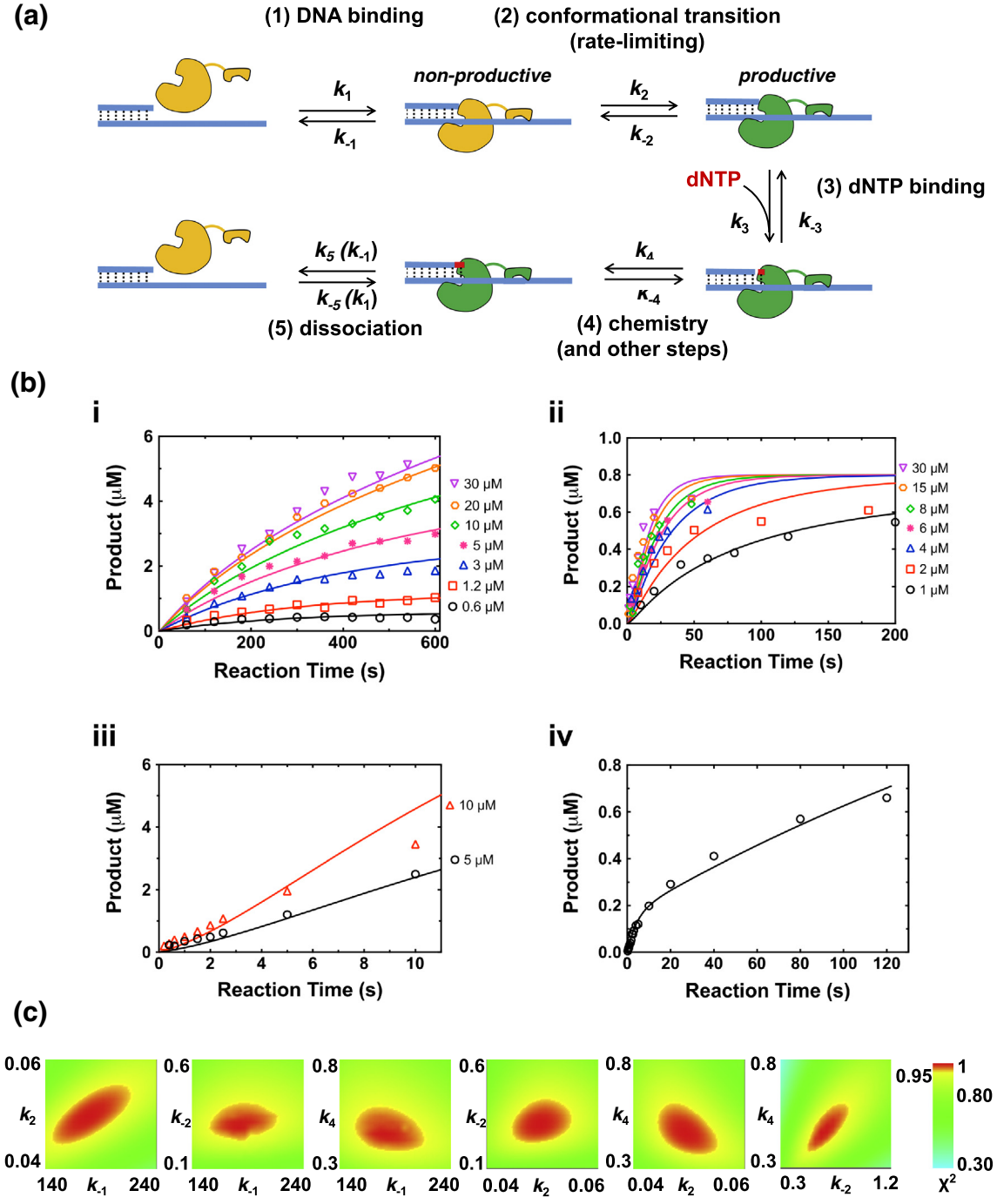

Fig. 5. Global data fitting and simulations of single-nucleotide extension by PrimPol. (a) Proposed kinetic mechanism for PrimPol-catalyzed nucleotidyl transfer. (b) Global fitting of data obtained with 2 mM Mn^{2+} to the kinetic model, including (i) steady-state kinetics, (ii) single-turnover kinetics, (iii) burst kinetics, and (iv) biphasic kinetics. (c) Fitspace contour analysis demonstrates the simulated rate constants are well constrained by the data. Contour plots show k_{-1}, k_2, k_{-2}, and k_4 as a function of each other. The boundary of each parameter is calculated when χ^2 threshold limit is set at 0.95.

comprising DNA binding (step 1), conformational transition (step 2), dNTP binding (step 3), phosphoester bond formation (step 4), and dissociation (step 5) steps, as shown in Fig. 5a. By simultaneously fitting multiple data sets to the proposed model, we evaluated the model and determined the kinetic constants of steps 2 and 4. The computer simulation methods have been proven to be powerful in extracting rate constants that are difficult to measure experimentally [39,47,48]. First, we globally fit the data from 2 mM Mn^{2+} reactions to the proposed kinetic model (Fig. 5b). Several kinetic constants were locked on the basis of empirical and experimental evidence. The on-rates for DNA binding (k_1) and nucleotide binding (k_3) were presumed to be diffusion limited (100–1000 μM^{-1} s^{-1}). The ratio of k_{-3}/k_3 was locked on the basis of the experimentally determined $K_{d,dTTP}$. The reverse rate constant of step 4 (k_{-4}) was set at 0.001 s^{-1} judging from the slow rate of pyrophosphorylation (see Supplemental Data for details). The concentration of the productive complexes was calculated according to the biphasic kinetic experiment (16% of the enzyme concentration, Table 3).

Global data fitting demonstrates that the proposed five-step kinetic model largely correlates with our experimental data (Fig. 5b). As summarized in Table 4, the simulated off-rate of PrimPol:DNA non-productive complexes (k_{-1}) is 180 s^{-1}, in agreement with the estimated lower limit of k_{-1} (200 s^{-1}) from a trap experiment (described in Supplemental Data). The fast dissociation from DNA is also consistent with the distributive characteristics of PrimPol [49]. The simulated forward (k_2) and reverse (k_{-2}) rates of the conformational transition are 0.050 and 0.29 s^{-1}, respectively, suggesting that two types of PrimPol:DNA complexes exist as an equilibrating mixture. The forward rate of step 4 (k_4, 0.46 s^{-1}) is 10-fold higher than k_{cat} (0.05 s^{-1}), corroborating a non-rate-limiting chemical step. On the other hand, k_2 is on the order of k_{cat} and is slower than k_4, confirming a rate-limiting conformational transition. Furthermore, we used confidence contour analysis to estimate the errors associated with the simulation and to reveal complex relationships between the simulated constants [50]. The resulting confidence contours demonstrate that the simulated parameters are well constrained by the data (Fig. 5c). Moreover, we explored the possibility of PrimPol forming productive complexes directly and proposed an alternative kinetic model including such a step (Fig. S5). We found that the formation rate of the productive complexes (0.024 μM^{-1} s^{-1})—formed upon PrimPol-DNA binding rather than being converted from nonproductive complexes—is 5 orders of magnitude lower than the competitive reaction to form non-productive complexes (Table S2). Therefore, we conclude that PrimPol is unlikely to form productive PrimPol:DNA complexes directly under the current experimental condition.

In addition, we performed the kinetic modeling with data from 2 mM Mg^{2+} or 50 μM Mn^{2+} experiments. We used the experimentally obtained $K_{d,DNA}$ value and the presumed k_1 to calculate k_{-1} ($K_{d,DNA}/k_1$) and to reduce the number of unknowns. The lack of biphasic kinetic data under these conditions precluded estimation of the relative proportions of productive and non-productive complexes; nonetheless, we performed simulations under different conditions, that is, productive complexes at 0, 25%, 50%, 75%, and 100% of the total enzyme, to cover the entire possible range. For Mg^{2+}-dependent reactions (Table S3 and Fig. S6), when productive complexes are assumed to be 0, 25%, 50%, or 75%, global fitting and simulations revealed that k_2 and k_4 are reasonably well constrained, whereas k_{-2} is not well constrained in some cases. Under these assumptions, the simulated k_4 values (~ 0.04 s^{-1}) are much lower than k_2 (ranges from 0.23 to 0.50 s^{-1}). When the productive complex is set at 100%, the k_2 value demonstrates a wide range, indicating that it is not well constrained by the data and the assumption is not consistent with the data. Collectively, the well-constrained k_4 and k_2 values confirm a rate-limiting chemical step for Mg^{2+}-dependent reactions.

For data with 50 μM Mn^{2+} (Table S4 and Fig. S7), kinetic simulation revealed that k_{-2} is not well defined by the data, as illustrated by the relatively wide range of values. On other hand, k_2 is well constrained under all assumptions and has a similar range of values compared to k_2 obtained from global fitting of 2 mM Mn^{2+} data. The observation confirms that the rate of conformational transition is comparable under different manganese concentrations. k_4 is well constrained when the productive

Table 4. Summary of kinetic constants for PrimPol-catalyzed nucleotide incorporation derived from the global data fitting

	k_1 (μM^{-1} s^{-1})	k_{-1} (s^{-1})	k_2 (s^{-1})	k_{-2} (s^{-1})	k_3 (μM^{-1} s^{-1})	k_{-3} (s^{-1})	k_4 (s^{-1})	k_{-4} (s^{-1})
2 mM Mn^{2+}								
Locked	1000				100	500		0.001
Simulated		180 (150–210)	0.050 (0.045–0.055)	0.29 (0.22–0.39)			0.46 (0.38–0.59)	

The lower and upper limits of each rate constant from confidence contour analysis are indicated in the parenthesis. Contour plots are shown in Fig. 5c.

complexes are assumed to be 100%, 75%, or 50%. Under such conditions, the upper limits of the simulated k_2 values are smaller than the lower limits of k_4, indicative of a rate-limiting conformational transition step under micromolar Mn^{2+}. Taken together, the combined data from kinetic experiments and simulations demonstrate the important role of divalent metal ions in altering the rate-limiting step of PrimPol-mediated phosphoryl-transfer reaction.

Discussion

Considering PrimPol as a specialized DNA polymerase

Specialized DNA polymerases play an important role in genomic maintenance and can adopt various strategies to physically accommodate DNA modifications or secondary structures [4–8]. Although the biological importance of PrimPol-mediated lesion bypass remains to be established *in vivo*, biochemical experiments have shown that PrimPol is able to traverse common DNA lesions, such as 8-oxo-7,8-dihydro-2′-deoxyguanosine and pyrimidine-pyrimidone (6–4) photoproducts [12,13,23]. Structural data revealed that PrimPol's active site is relatively constrained with respect to the template nucleotide compared to that of pol η (an important DNA polymerase to counteract UV-induced DNA damage) [26]. It is conceivable that PrimPol uses different tactics to bypass distorting lesions, such as the "looping-out" mechanism proposed previously [33]. Kinetic analysis complements the structural studies and provides a wealth of knowledge on the elementary steps of catalysis [38,51,52]. A typical DNA polymerization reaction includes microscopic steps, such as DNA binding, dNTP binding, conformational change, phosphoryl transfer, and pyrophosphate dissociation. However, individual DNA polymerases differ considerably in the relative stabilities of enzyme-bound intermediates and consequently in the rates of microscopic steps of the reaction [51].

The kinetic mechanism of PrimPol-catalyzed DNA elongation had remained an important unsolved question. In this study, we have elucidated the kinetic basis of PrimPol using enzyme kinetic assays and computer simulations. Our data demonstrate unambiguously that PrimPol exhibits a rate-limiting step at or prior to the chemical step depending on the metal cofactor present. Key experimental evidence for the conclusion includes the lack of burst kinetics (Fig. 2), distinct thio-effects under different metal cofactors (Figs. 3, S3, and S4, and Table 2), biphasic kinetics under millimolar Mn^{2+} (Fig. 4 and Table 3), and the simulated rate constants from global data fitting (Figs. 5, S6, and S7, and Tables 4, S3, and S4). PrimPol's lack of burst kinetics is reminiscent of B-family pol α [53] but is different from most other DNA polymerases, which possess a burst kinetic profile due to a rate-limiting step occurring after the chemical step [38,48,51,52].

Consistent with our observations, Tokarsky *et al.* [28] had proposed that PrimPol lacks a burst product formation. On the other hand, Mislak and Anderson [27] reported burst kinetics for PrimPol. The discrepancy may arise from the higher metal concentration (10 mM Mn^{2+}) and the different DNA substrate used in their study [27]. Also, the K_m values for two divalent metals we obtained are slightly higher compared to an earlier study [23], which is likely due to the different DNA substrates used, leading to different amounts of divalent cations associated with the phosphate group of DNA substrates [44]. We reason that in addition to the enzyme preparation itself, PrimPol's kinetic properties are influenced by the metal cofactors, DNA substrates, and other experimental conditions, such as the buffer, pH, the way reaction components are assembled, and the length of the reaction time.

Influence of divalent ions on PrimPol's catalysis

Our data suggest an important regulatory role of metal cofactors for PrimPol's enzyme kinetic characteristics. Compared to Mg^{2+}, Mn^{2+} stimulates DNA synthesis by DNA polymerases at the expense of fidelity [44,54]. The stimulatory effects of Mn^{2+} have been documented for a number of DNA polymerases, including bacteriophage T4 DNA polymerase [55], *Escherichia coli* DNA polymerase I [44], human pol ι [56], and human pol μ [40]. As for PrimPol, we demonstrate that Mn^{2+}-dependent reactions occur at a faster rate compared to those with Mg^{2+} mainly due to superior DNA and nucleotide binding and a faster phosphoryl-transfer rate (k_4 in Fig. 5a). Manganese may also contribute to the stabilization of a closed ternary complex, as suggested previously [54]. The net effect is that in the presence of Mn^{2+}, a conformational transition step before chemistry limits the enzymatic turnover. This is the case under both micromolar and millimolar Mn^{2+} concentrations, as evidenced from simulations. Judging from the 2-fold lower in k_{cat} with 50 μM Mn^{2+} relative to 2 mM Mn^{2+}, it may appear that the turnover number is lower under micromolar Mn^{2+}. However, the identical k_{pol} values under two conditions (Table 2) and similar k_4 values from simulations argue that the concentration of Mn^{2+} does not significantly alter PrimPol's kinetic pathway. We reason that a slightly lower k_{cat} value under 50 μM Mn^{2+} arises from the association of metal ions with the DNA substrate [44], which decreases the available metal ions for catalysis. The effect is more evident under steady-state experiments with 20 μM DNA than the single-turnover experiments with 0.8 μM DNA. Our kinetic data and simulations support the notion that Mn^{2+} can be a preferred metal cofactor for PrimPol [12,13,15,23,33], even under micromolar

Mn^{2+}. Considering that manganese is known to accumulate in brain and liver mitochondria [35,36] and that PrimPol potentially plays a role in mitochondrial DNA replication [13,20], it is conceivable that PrimPol's enzymatic activity can be stimulated by Mn^{2+} under certain conditions. A recent report focused on PrimPol's primase activity also supports in the importance of Mn^{2+} in forming pre-ternary complexes in PrimPol-mediated DNA priming [24].

Considering PrimPol as a primase

Primases are grouped into two evolutionarily unrelated classes: DnaG-like (bacteria) and AEP-like (archaea and eukaryotes) [57]. PrimPol is only the second human primase discovered to date with the first being Prim1, a subunit of the heterodimeric human primase [Prim1(p49):Prim2(p58)]. The Prim1 subunit possesses the primary active site for synthesizing RNA primers of 7–10 nt, whereas the Prim2 subunit plays an important regulatory role for the primase activity and primer transfer to pol α. Unlike Prim1, PrimPol has both primase and DNA-dependent DNA polymerase activities. PrimPol prefers dNTP substrates during primer elongation but favors NTP as the initiating 5′-nucleotide [24]. The turnover number (k_{cat}) of PrimPol-catalyzed dNTP incorporation is comparable to that of Prim1 with NTP [58]; however, larger $K_{m,dNTP}$ values observed for PrimPol result in an overall 20 to 40-fold lower catalytic proficiency relative to Prim1. Nonetheless, the ability of PrimPol to restart DNA synthesis from nonconventional origins and the fact that resulting DNA primers require no RNA processing may lend PrimPol advantages in DNA priming. Indeed, a growing body of studies corroborates the functional importance of PrimPol's primase activity in ensuring the fork progression in cells [13,15,16,19,20]. Although the current study does not directly address the kinetic steps during dinucleotide synthesis, the kinetic characteristics obtained here are pertinent to the elongation stage of PrimPol-catalyzed priming [24]. Additional studies are warranted to investigate the kinetic mechanism of PrimPol's primase activity.

AEP superfamily enzymes distributed across all domains of life [59]. Considering the diverse functions and evolutionary origins of AEP superfamily enzymes, it has been suggested to reclassify these enzymes under a category named primase-polymerases [59]. The dual enzymatic activities of PrimPol are reminiscent of certain PriS/PriL complexes observed in other archaea, including *Pyrococcus horikoshii* [60], *Sulfolobus solfactaricus* [61], *Thermococcus kodakaraensis* [62], and *Archaeoglobus fulgidus* [63] with varying abilities of using dNTP and NTP substrates. Other members of the AEP superfamily primases can also perform translesion DNA synthesis, such as the PriS subunit of archaeal replicative primases in *A. fulgidus* and *Pyrococcus furiosus* [63]. Further research is needed to establish the kinetic mechanism of other AEP enzymes and to compare and contrast with the kinetic pathway of PrimPol.

In conclusion, we report the first set of comprehensive kinetic analyses of the PrimPol-catalyzed nucleotide transfer, pertinent to PrimPol's DNA polymerase and primase activities. Our kinetic and simulation data elucidate the kinetic basis of PrimPol and emphasize the importance of metal cofactor for PrimPol's kinetic properties. Such knowledge contributes to the fundamental understanding of PrimPol and other primase-polymerase family enzymes.

Materials and Methods

Materials

Unless otherwise mentioned, all chemicals were the highest quality available purchased from Sigma-Aldrich (St. Louis, MO) or Research Products International (Mt Prospect, IL). 2′-Deoxythymidine triphosphate (dTTP) was from New England Biolabs (Ipswich, MA). The *S*p-isomer of 2′-deoxythymidine-5′-*O*-(1-thiotriphosphate) [(α)*S*-dTTP] (> 95% purity based on HPLC/UV analysis) was from BioLog (distributed by Axxora, LLC.). Unmodified oligodeoxynucleotides were synthesized and PAGE-purified by Integrated DNA Technologies (Coralville, IA) or TriLink Biotechnologies. Oligodeoxynucleotides with a 6-carboxyfluorescein (FAM) label at the 5′-end were HPLC purified. Expression and purification of PrimPol were performed as described previously [12] with modifications; the detailed procedure is described in Supplemental Data. The concentration of PrimPol was first determined by UV absorbance at 280 nm and corrected to the active PrimPol concentration (see Supplemental Data for details). The active PrimPol ranges from 70% to 90% of the total PrimPol concentration from different preparations (Fig. S1). All concentrations described in kinetic experiments are active PrimPol concentrations.

Multiple-turnover kinetics

Primer-template DNA substrates were prepared by annealing FAM-labeled 13-mer oligomer primer (DNA-13) to a 28-mer (DNA-28) or 73-mer oligomer (DNA-73) template at a 1:1 molar ratio (sequences shown in Table S1 of the Supplemental Data). All DNA polymerization reactions were carried out in a reaction buffer containing 50 mM Hepes at pH 7.4 (37 °C), 50 mM NaCl, 5% glycerol, 100 μg/mL BSA, and 5 mM β-mercaptoethanol. Reaction components (buffer, DNA, and PrimPol) were assembled on ice and equilibrated for 2 min at 37 °C prior to the addition of 200 μM dTTP and 2 mM $MnCl_2$ (or $MgCl_2$) for

polymerization. All concentrations are final concentrations in the reaction. Reactions were quenched by mixing a 1.5-μL aliquot of the mixture with 8.5 μL of 95% (v/v) formamide/50 mM EDTA solution. Reaction products were resolved by 16% denaturing-PAGE with 7 M urea. To evaluate the enzyme stability, salt, DNA, and metal concentration dependencies, multiple-turnover assays were conducted in the presence of 20 μM annealed primer-template DNA and 100 nM PrimPol for varying times. Steady-state kinetic analysis was carried out with 20 μM annealed primer-template DNA and 100 nM PrimPol (for DNA-13/28) or 600 nM PrimPol (for DNA-13/73) for varying times. The burst kinetic assays were performed on a rapid quench apparatus (RQF-3; KinTek Corporation, Snow Shoe, PA) at 37 °C. Syringe A contained 60 μM annealed primer-template DNA and 20 μM (or 130 μM) PrimPol, and syringe B contained 400 μM dTTP and 4 mM $MnCl_2$. Reaction components in both syringes were in the DNA polymerization reaction buffer. The reaction was initiated by mixing a 20-μL aliquot from each syringe and quenched at varying times using 0.3 M EDTA. Under these conditions, more than 99% of the PrimPol molecules were saturated with DNA on the basis of $K_{d,DNA}$, calculated from Eq. (7) (*vide infra*). Reaction products were precipitated with ethanol (in the presence of 3 mg mL^{-1} of carrier salmon sperm DNA) and resuspended in 95% (*v*/v) formamide/50 mM EDTA solution for gel electrophoretic analysis.

Single-turnover kinetics

Single-turnover assays were carried out with the RQF-3 rapid quench apparatus at 37 °C. Syringe A contained 1.6 μM FAM-labeled primer-template DNA and 8 μM PrimPol; syringe B contained varying concentrations of dTTP and 4 mM $MnCl_2$. Components from both syringes were mixed and allowed for varying reaction times followed by quenching with 0.3 M EDTA. Reactions with (α)*S*-dTTP in the presence of 2 mM or 50 μM Mn^{2+} were performed under the same conditions, except that the mixing of reaction components was done manually. In the presence of 1.6 μM FAM-labeled primer-template DNA and 8 μM PrimPol, more than 95% of the PrimPol molecules were saturated to form PrimPol:DNA complexes according to $K_{d,DNA}$. DNA trapping experiments were performed using the rapid quench apparatus with 2 μM FAM-labeled primer-template DNA and 4 μM PrimPol in one syringe and 400 μM dTTP, 4 mM Mn^{2+}, and 70 μM unlabeled primer-template DNA (DNA-16/23) trap in the other syringe. Under this condition, the concentration of PrimPol:FAM-DNA complexes is 0.8 μM on the basis of $K_{d,DNA}$; the remaining 1.2 μM of unbound PrimPol was trapped by the unlabeled DNA upon the addition of DNA-16/23.

Conventional data analysis

Gel imaging was performed on a Typhoon FLA7000 (GE Healthcare) imager, and results were quantified using ImageQuant software. Data were analyzed using nonlinear regression (GraphPad Prism v6.0). The apparent equilibrium dissociation constant ($K_{d,DNA}$) of DNA:PrimPol binary complex was obtained by fitting the change of polarization as a function of PrimPol concentration to a quadratic equation

$$y = F + \frac{D \times (P-F) \times \left[K_{d,DNA} + x + D - \sqrt{(K_{d,DNA} + x + D)^2 - 4Dx}\right]}{2} \quad (1)$$

where y is the change of fluorescence polarization, x is PrimPol concentration, D is DNA concentration, P is the maximal polarization, and F is the initial polarization.

The half-life of PrimPol under different conditions was estimated by fitting DNA polymerase activity as a function of time to the following equation

$$k_{obsm} = (k_{obs,m_{max}} - k_{obs,m_{min}}) \times e^{-kt} + k_{obs,m_{min}} \quad (2)$$

where $k_{obs,m}$ is calculated from the initial DNA polymerization rate divided by enzyme concentration (V_0/[E]) and t is the reaction time.

The steady-state kinetic parameters k_{cat} and K_m were obtained by fitting data to the Michaelis–Menten equation, where k_{obs} is calculated from the initial reaction rate divided by enzyme concentration.

$$k_{obs} = \frac{k_{cat} \times [S]}{K_m + [S]} \quad (3)$$

Time-dependent product formation under single-turnover conditions was fit to a single-exponential equation

$$[\text{Product}] = A \times \left(1 - e^{-k_{obs,s}t}\right) \quad (4)$$

where A is the product amplitude following the first binding event, and t is the reaction time. The maximal nucleotidyl-transfer rate constant k_{pol} and the apparent equilibrium dissociation constant of nucleotide ($K_{d,dNTP}$) were obtained with equation

$$k_{obs,s} = \frac{k_{pol} \times [dTNP]}{K_{d,dTNP} + [dTNP]} \quad (5)$$

The biphasic kinetics was fit to a double-exponential equation

$$[\text{Product}] = A_{fast} \times \left(1 - e^{-k_{fast}t}\right) + A_{slow} \times \left(1 - e^{-k_{slow}t}\right) \quad (6)$$

where A is the product amplitude in each phase, and t is the reaction time. The concentration of E:DNA complex was calculated on the basis of $K_{d,DNA}$ using a quadratic equation

$$[E \cdot D] = \frac{K_{d,DNA} + [E_0] + [D_0] - \sqrt{(K_{d,DNA} + [E_0] + [D_0])^2 - 4 \times [E_0] \times [D_0]}}{2} \quad (7)$$

where $[E_0]$ is the enzyme concentration, $[D_0]$ is the DNA concentration, and $K_{d,DNA}$ is the equilibrium dissociation constant.

Global fitting and computer simulation

Results from steady-state, pre-steady burst, single-turnover, and DNA trapping experiments were fit globally to a four-step kinetic model (Fig. 5a) using KinTek Explorer 7 software [47]. Concentrations of reaction components were input as equilibrium concentrations including complexes and free reactants. Initial values of kinetic parameters were estimated by conventional data analysis. All the on-rates were presumed to be diffusion-limited (1×10^8–1×10^9 M^{-1} s^{-1}), while all the other parameters were allowed to vary. From the initial fitting result, we found several parameters (k_{-1}, k_2, k_{-2}, k_4, and k_{-4}) distributed in a wide range with a maximum. The rate constant of pyrophosphorylation was lower than 5×10^{-5} μM^{-1} s^{-1} (see Supplemental Data for details). Based on the simulated upper limit, k_{-4} was locked at 0.001 during global fitting. When k_3 was fixed at 100 μM^{-1} s^{-1}, the dissociation rate of PrimPol•DNA was much smaller than the estimated minimal rate of 200 s^{-1} (see Supplemental Data for details). Thus, k_1 was locked at 1000 (μM^{-1} s^{-1}), a reasonable presumption for the diffusion-limited processes. FitSpace Explorer was utilized to evaluate the reliability of fit [50]. The χ^2 threshold limit was set at 0.8 for fitting. The lower bound and upper bound of parameters were obtained by setting χ^2 threshold at bound as 0.95. The FitSpace confidence contours demonstrate that data were well constrained by the proposed kinetic model and experimental data. An alternative model with an additional step that PrimPol binds to DNA to directly form productive PrimPol:DNA complexes was explored during global fitting analysis, but was not adopted considering the extremely slow formation of such complexes (described in the Supplemental Data).

Acknowledgments

This work was supported by US National Institutes of Health grant R15 GM117522 (to L.Z.). The content is solely the responsibility of the authors and does not necessarily represent the official views of the National Institutes of Health. We thank Dr. Marc S. Wold for critically reading the manuscript.

Conflict of interest: The authors declare that they have no conflicts of interest with the contents of this article.

Appendix A. Supplementary Data

This article contains supplemental methods and supplemental data Tables S1–S4 and Figs. S1–S8. Supplementary data to this article can be found online at https://doi.org/10.1016/j.jmb.2019.01.002.

Received 28 August 2018;
Received in revised form 20 December 2018;
Accepted 2 January 2019
Available online 8 January 2019

Keywords:
enzyme mechanism;
enzymology;
enzyme kinetics;
DNA polymerase;
DNA replication

Abbreviations used:
AEP, archaeo-eukaryotic primase; (α)*S*-dTTP, *S*p-isomer of 2′-deoxythymidine-5′-*O*-(1-thiotriphosphate); FAM, 6-carboxyfluorescein; pol, DNA polymerase.

References

[1] J.H.J. Hoeijmakers, Genome maintenance mechanisms for preventing cancer, Nature 411 (2001) 366–374.
[2] F.P. Guengerich, L. Zhao, M.G. Pence, M. Egli, Structure and function of the translesion DNA polymerases and interactions with damaged DNA, Perspect. Sci. 4 (2015) 24–31.
[3] I. Saugar, M.Á. Ortiz-Bazán, J.A. Tercero, Tolerating DNA damage during eukaryotic chromosome replication, Exp. Cell Res. 329 (2014) 170–177.
[4] E.C. Friedberg, R. Wagner, M. Radman, Specialized DNA polymerases, cellular survival, and the genesis of mutations, Science 296 (2002) 1627–1630.
[5] J.E. Sale, Translesion DNA synthesis and mutagenesis in eukaryotes, Cold Spring Harb. Perspect. Biol. 5 (2013) a012708.
[6] W. Yang, R. Woodgate, What a difference a decade makes: insights into translesion DNA synthesis, Proc. Natl. Acad. Sci. U. S. A. 104 (2007) 15591–15598.
[7] L.S. Waters, B.K. Minesinger, M.E. Wiltrout, S. D'Souza, R.V. Woodruff, G.C. Walker, Eukaryotic translesion polymerases and their roles and regulation in DNA damage tolerance, Microbiol. Mol. Biol. Rev. 73 (2009) 134–154.
[8] J.E. Sale, A.R. Lehmann, R. Woodgate, Y-family DNA polymerases and their role in tolerance of cellular DNA damage, Nat. Rev. Mol. Cell Biol. 13 (2012) 141–152.

[9] A.V. Makarova, P.M. Burgers, Eukaryotic DNA polymerase ζ, DNA Repair 29 (2015) 47–55.
[10] Y.-S. Lee, M.T. Gregory, W. Yang, Human Pol ζ purified with accessory subunits is active in translesion DNA synthesis and complements Pol η in cisplatin bypass, Proc. Natl. Acad. Sci. U. S. A. 111 (2014) 2954–2959.
[11] L. Zhao, T.M. Washington, Translesion synthesis: insights into the selection and switching of DNA polymerases, Genes 8 (2017) 24.
[12] J. Bianchi, S.G. Rudd, S.K. Jozwiakowski, L.J. Bailey, V. Soura, E. Taylor, et al., PrimPol bypasses UV photoproducts during eukaryotic chromosomal DNA replication, Mol. Cell 52 (2013) 566–573.
[13] S. García-Gómez, A. Reyes, M.I. Martínez-Jiménez, E.S. Chocrón, S. Mourón, G. Terrados, et al., PrimPol, an archaic primase/polymerase operating in human cells, Mol. Cell 52 (2013) 541–553.
[14] T. Helleday, PrimPol breaks replication barriers, Nat. Struct. Mol. Biol. 20 (2013) 1348–1350.
[15] S. Mourón, S. Rodriguez-Acebes, M.I. Martínez-Jiménez, S. García-Gómez, S. Chocrón, L. Blanco, et al., Repriming of DNA synthesis at stalled replication forks by human PrimPol, Nat. Struct. Mol. Biol. 20 (2013) 1383–1389.
[16] L. Wan, J. Lou, Y. Xia, B. Su, T. Liu, J. Cui, et al., hPrimpol1/CCDC111 is a human DNA primase-polymerase required for the maintenance of genome integrity, EMBO Rep. 14 (2013) 1104–1112.
[17] S.G. Rudd, L. Glover, S.K. Jozwiakowski, D. Horn, A.J. Doherty, PPL2 translesion polymerase is essential for the completion of chromosomal DNA replication in the African trypanosome, Mol. Cell 52 (2013) 554–565.
[18] E.O. Boldinova, P.H. Wanrooij, E.S. Shilkin, S. Wanrooij, A.V. Makarova, DNA damage tolerance by eukaryotic DNA polymerase and primase PrimPol, Int. J. Mol. Sci. 18 (2017) 1584.
[19] D. Schiavone, S.K. Jozwiakowski, M. Romanello, G. Guilbaud, T.A. Guilliam, L.J. Bailey, et al., PrimPol is required for replicative tolerance of G quadruplexes in vertebrate cells, Mol. Cell 61 (2016) 161–169.
[20] R. Torregrosa-Muñumer, J.M. Forslund, S. Goffart, A. Pfeiffer, G. Stojkovič, G. Carvalho, et al., PrimPol is required for replication reinitiation after mtDNA damage, Proc. Natl. Acad. Sci. U. S. A. 114 (2017) 11398–11403 (201705367).
[21] K. Kobayashi, T.A. Guilliam, M. Tsuda, J. Yamamoto, L.J. Bailey, S. Iwai, et al., Repriming by PrimPol is critical for DNA replication restart downstream of lesions and chain-terminating nucleosides, Cell Cycle 15 (2016) 1997–2008.
[22] B. Pilzecker, O.A. Buoninfante, C. Pritchard, O.S. Blomberg, I.J. Huijbers, P.C. van den Berk, et al., PrimPol prevents APOBEC/AID family mediated DNA mutagenesis, Nucleic Acids Res. 44 (2016) 4734–4744.
[23] M.K. Zafar, A. Ketkar, M.F. Lodeiro, C.E. Cameron, R.L. Eoff, Kinetic analysis of human PrimPol DNA polymerase activity reveals a generally error-prone enzyme capable of accurately bypassing 7, 8-dihydro-8-oxo-2′-deoxyguanosine, Biochemistry 53 (2014) 6584–6594.
[24] M.I. Martínez-Jiménez, P.A. Calvo, S. García-Gómez, S. Guerra-González, L. Blanco, The Zn-finger domain of human PrimPol is required to stabilize the initiating nucleotide during DNA priming, Nucleic Acids Res. 46 (2018) 4138–4151.
[25] T.A. Guilliam, N.C. Brissett, A. Ehlinger, B.A. Keen, P. Kolesar, E.M. Taylor, et al., Molecular basis for PrimPol recruitment to replication forks by RPA, Nat. Commun. 8 (2017), 15222.
[26] O. Rechkoblit, Y.K. Gupta, R. Malik, K.R. Rajashankar, R.E. Johnson, L. Prakash, et al., Structure and mechanism of human PrimPol, a DNA polymerase with primase activity, Sci. Adv. 2 (2016), e1601317.
[27] A.C. Mislak, K.S. Anderson, Insights into the molecular mechanism of polymerization and nucleoside reverse transcriptase inhibitor incorporation by human PrimPol, Antimicrob. Agents Chemother. 60 (2016) 561–569.
[28] E.J. Tokarsky, P.C. Wallenmeyer, K.K. Phi, Z. Suo, Significant impact of divalent metal ions on the fidelity, sugar selectivity, and drug incorporation efficiency of human PrimPol, DNA Repair 49 (2017) 51–59.
[29] R. Agudo, P.A. Calvo, M.I. Martínez-Jiménez, L. Blanco, Engineering human PrimPol into an efficient RNA-dependent-DNA primase/polymerase, Nucleic Acids Res. 45 (2017) 9046–9058.
[30] A.J. Picher, B. Budeus, O. Wafzig, C. Krüger, S. García-Gómez, M.I. Martínez-Jiménez, et al., TruePrime is a novel method for whole-genome amplification from single cells based on TthPrimPol, Nat. Commun. 7 (2016), 13296.
[31] E. Gasteiger, C. Hoogland, A. Gattiker, M.R. Wilkins, R.D. Appel, A. Bairoch, Protein identification and analysis tools on the ExPASy server, The Proteomics Protocols Handbook, Springer 2005, pp. 571–607.
[32] E.O. Boldinova, G. Stojkovič, R. Khairullin, S. Wanrooij, A.V. Makarova, Optimization of the expression, purification and polymerase activity reaction conditions of recombinant human PrimPol, PLoS One 12 (2017), e0184489.
[33] M.I. Martínez-Jiménez, S. García-Gómez, K. Bebenek, G. Sastre-Moreno, P.A. Calvo, A. Díaz-Talavera, et al., Alternative solutions and new scenarios for translesion DNA synthesis by human PrimPol, DNA Repair 29 (2015) 127–138.
[34] D.G. Kehres, M.E. Maguire, Emerging themes in manganese transport, biochemistry and pathogenesis in bacteria, FEMS Microbiol. Rev. 27 (2003) 263–290.
[35] L.S. Maynard, G.C. Cotzias, The partition of manganese among organs and intracellular organelles of the rat, J. Biol. Chem. 214 (1955) 489–495.
[36] C.E. Gavin, K.K. Gunter, T.E. Gunter, Manganese and calcium efflux kinetics in brain mitochondria. Relevance to manganese toxicity, Biochem. J. 266 (1990) 329–334.
[37] A.M. Romani, Cellular magnesium homeostasis, Arch. Biochem. Biophys. 512 (2011) 1–23.
[38] M.P. Roettger, M. Bakhtina, S. Kumar, M.-D. Tsai, 8.10—catalytic mechanism of DNA polymerases, in: H.-W. Liu, L. Mander (Eds.), Comprehensive Natural Products II, Elsevier, Oxford 2010, pp. 349–383.
[39] A.S.P. Gowda, G.-L. Moldovan, T.E. Spratt, Human DNA polymerase v catalyzes correct and incorrect DNA synthesis with high catalytic efficiency, J. Biol. Chem. 290 (2015) 16292–16303.
[40] J.A. Jamsen, W.A. Beard, L.C. Pedersen, D.D. Shock, A.F. Moon, J.M. Krahn, et al., Time-lapse crystallography snapshots of a double-strand break repair polymerase in action, Nat. Commun. 8 (2017) 253.
[41] J.-Y. Choi, F.P. Guengerich, Analysis of the effect of bulk at N2-alkylguanine DNA adducts on catalytic efficiency and fidelity of the processive DNA polymerases bacteriophage T7 exonuclease-and HIV-1 reverse transcriptase, J. Biol. Chem. 279 (2004) 19217–19229.
[42] K.A. Johnson, Conformational coupling in DNA polymerase fidelity, Annu. Rev. Biochem. 62 (1993) 685–713.

[43] A.K. Showalter, M.-D. Tsai, A reexamination of the nucleotide incorporation fidelity of DNA polymerases, Biochemistry 41 (2002) 10571–10576.
[44] R.A. Beckman, A.S. Mildvan, L.A. Loeb, On the fidelity of DNA replication: manganese mutagenesis in vitro, Biochemistry 24 (1985) 5810–5817.
[45] Z. Suo, K.A. Johnson, DNA secondary structure effects on DNA synthesis catalyzed by HIV-1 reverse transcriptase, J. Biol. Chem. 273 (1998) 27259–27267.
[46] K.D. Carlson, R.E. Johnson, L. Prakash, S. Prakash, M.T. Washington, Human DNA polymerase κ forms nonproductive complexes with matched primer termini but not with mismatched primer termini, Proc. Natl. Acad. Sci. U. S. A. 103 (2006) 15776–15781.
[47] K.A. Johnson, Z.B. Simpson, T. Blom, Global Kinetic Explorer: a new computer program for dynamic simulation and fitting of kinetic data, Anal. Biochem. 387 (2009) 20–29.
[48] L. Zhao, M.G. Pence, R.L. Eoff, S. Yuan, C.A. Fercu, F.P. Guengerich, Elucidation of kinetic mechanisms of human translesion DNA polymerase κ using tryptophan mutants, FEBS J. 281 (2014) 4394–4410.
[49] B.A. Keen, S.K. Jozwiakowski, L.J. Bailey, J. Bianchi, A.J. Doherty, Molecular dissection of the domain architecture and catalytic activities of human PrimPol, Nucleic Acids Res. 42 (2014) 5830–5845.
[50] K.A. Johnson, Z.B. Simpson, T. Blom, FitSpace Explorer: an algorithm to evaluate multidimensional parameter space in fitting kinetic data, Anal. Biochem. 387 (2009) 30–41.
[51] C.M. Joyce, Techniques used to study the DNA polymerase reaction pathway, Biochim. Biophys. Acta Proteins Proteomics 1804 (2010) 1032–1040.
[52] M.T. Washington, K.D. Carlson, B.D. Freudenthal, J.M. Pryor, Variations on a theme: eukaryotic Y-family DNA polymerases, Biochim. Biophys. Acta Protein Proteomics 1804 (2010) 1113–1123.
[53] A.G. Baranovskiy, V.N. Duong, N.D. Babayeva, Y. Zhang, Y.I. Pavlov, K.S. Anderson, et al., Activity and fidelity of human DNA polymerase α depend on primer structure, J. Biol. Chem. 293 (2018) 6824–6843.
[54] A.K. Vashishtha, J. Wang, W.H. Konigsberg, Different divalent cations alter the kinetics and fidelity of DNA polymerases, J. Biol. Chem. 291 (2016) 20869–20875 (jbc. R116. 742494).
[55] H. Hays, A.J. Berdis, Manganese substantially alters the dynamics of translesion DNA synthesis, Biochemistry 41 (2002) 4771–4778.
[56] E.G. Frank, R. Woodgate, Increased catalytic activity and altered fidelity of human DNA polymerase ι in the presence of manganese, J. Biol. Chem. 282 (2007) 24689–24696.
[57] D.N. Frick, C.C. Richardson, DNA primases, Annu. Rev. Biochem. 70 (2001) 39–80.
[58] M. Urban, N. Joubert, B.W. Purse, M. Hocek, R.D. Kuchta, Mechanisms by which human DNA primase chooses to polymerize a nucleoside triphosphate, Biochemistry 49 (2010) 727–735.
[59] T.A. Guilliam, B.A. Keen, N.C. Brissett, A.J. Doherty, Primase-polymerases are a functionally diverse superfamily of replication and repair enzymes, Nucleic Acids Res. 43 (2015) 6651–6664.
[60] E. Matsui, M. Nishio, H. Yokoyama, K. Harata, S. Darnis, I. Matsui, Distinct domain functions regulating de novo DNA synthesis of thermostable DNA primase from hyperthermophile *Pyrococcus horikoshii*, Biochemistry 42 (2003) 14968–14976.
[61] S.-h. Lao-Sirieix, S.D. Bell, The heterodimeric primase of the hyperthermophilic archaeon Sulfolobus solfataricus possesses DNA and RNA primase, polymerase and 3′-terminal nucleotidyl transferase activities, J. Mol. Biol. 344 (2004) 1251–1263.
[62] W.C. Galal, M. Pan, Z. Kelman, J. Hurwitz, Characterization of DNA primase complex isolated from the archaeon, *Thermococcus kodakaraensis*, J. Biol. Chem. 287 (2012) 16209–16219.
[63] S.K. Jozwiakowski, F.B. Gholami, A.J. Doherty, Archaeal replicative primases can perform translesion DNA synthesis, Proc. Natl. Acad. Sci. U. S. A. 112 (2015) E633–E638.